JOURNAL OF CATALYSIS 85, 143–153 (1984)

Influence of Adsorption and Mass Transfer Effects on Temperature-Programmed Desorption from Porous Catalysts

JEFFERY S. RIECK AND ALEXIS T. BELL

Materials and Molecular Research Division, Lawrence Berkeley Laboratory, and Department of Chemical Engineering, University of California, Berkeley, California 94720

Received May 12, 1983; revised August 1, 1983

A theoretical analysis is presented for temperature-programmed desorption (TPD) from a bed of catalyst perfused by a flow of carrier gas. The bed is modeled either as a single CSTR or as multiple CSTR's connected in series. The number of CSTR's required is governed by the product of Schmidt and Reynold's number, *ScRe*. The model developed in this paper is used to calculate TPD spectra for the desorption of CO and H_2 from the surface of a Group VIII metal. It is established that the position and shape of the spectra are sensitive functions of catalyst particle size, catalyst bed depth, carrier flow rate, and carrier gas composition. The effects of nonuniformities in the initial distribution of adsorbate are also examined. For small particle diameters, such nonuniformities are rapidly annealed by intraparticle diffusion, and as a consequence have little effect on the shape or position of the TPD spectrum. For larger particle diameters, distortions of the spectrum due to nonuniform adsorbate distribution are expected. The theoretically generated TPD spectra are used to evaluate the applicability of a relationship developed for describing equilibrium desorption in the absence of mass transfer effects. Reasonably accurate estimates of the enthalpy of adsorption can be obtained from this relationship, but its use to determine the preexponential factor for desorption produces large errors when significant mass transfer effects are present.

INTRODUCTION

Temperature-programmed desorption (TPD) spectra obtained from porous supported catalysts can be strongly influenced by the effects of gas readsorption and diffusional mass transfer, as well as by the intrinsic kinetics of desorption (*1–6*). As a consequence, the interpretation of such spectra to determine the order and rate parameters for desorption of a given species is more difficult than for the case of desorption from nonporous samples, such as single crystals, films, and foils. Two recent efforts have analyzed the problem of TPD from porous samples, with the aim of establishing the influence of readsorption and mass transport effects on the position and shape of TPD peaks for a first-order desorption process. Herz *et al.* (*3*) have carried out an analysis for CO desorption from a thin wafer of supported Pt, both into a carrier gas and into vacuum. Their results indicate that for conditions representative of those used in experiments with supported Group VIII metals, adsorption effects cannot be neglected, and that adsorption equilibrium is closely approached at each point in the sample. Significant gradients in the concentration of CO within the sample were predicted for thick samples and high gas flow rates (desorption into a vacuum). By nondimensionalizing the equations used in the model given by Herz *et al.* (*3*), Gorte (*4*) has been able to characterize the problem in terms of four dimensionless groups. The magnitude of these groups determine which physical phenomena are most important. Gorte (*4*) concluded that concentration gradients within the sample can be eliminated by appropriate selection of sample thickness and carrier flow rate. Readsorption, however, cannot be eliminated for any reasonable combination of conditions. It was also demonstrated that the lag time for sample measurement and the lag

0021-9517/84 $3.00

time for gas to diffuse out of the pores can be made negligibly small, thereby eliminating any complications due to lag times.

This paper presents an analysis for TPD from a bed of catalyst perfused by a flow of carrier gas, a configuration used frequently in experimental studies of TPD from porous catalysts (*6*). Consideration is given to the influence of carrier flow rate, carrier composition, catalyst particle size, and catalyst bed depth for both first- and second-order desorption processes. The influence of spatially nonuniform adsorption is also examined. The theoretically generated TPD spectra are then analyzed in the light of theory developed for the case of equilibrium readsorption, in the absence of intraparticle or interparticle mass-transfer effects. The purpose of this phase of the work is to establish the extent to which the equation, describing peak position as a function of heating rate, can be used to determine the activation energy and preexponential factor for desorption.

THEORY

Temperature-programmed desorption is taken to occur from a fixed bed of catalyst into a flowing carrier gas that passes through the bed. The bed is modeled either as a single Continuously Stirred Tank Reactor (CSTR) (*7*) or as a series of smaller CSTR's, as shown in Fig. 1. Within each CSTR, the gas composition in the voids between individual catalyst particles is assumed to be constant. The number of CSTR's required to describe the behavior of the bed properly depends on the extent of axial dispersion. For a fixed bed of particles, the distance over which a portion of the bed can be treated as a CSTR is given by (*7*)

$$\frac{\Delta z}{D_p} = \frac{2}{Pe} = \frac{0.6}{ScRe} + \frac{1}{[1 + 3.8/(ScRe)]} \tag{1}$$

where

$$ScRe = \frac{\bar{u}D_p}{\mathcal{D}} \tag{2}$$

Definitions of the parameters and variables appearing in Eqs. (1) and (2) are given in the Appendix.

A plot of Eq. (1) is presented in Fig. 2. At high values of $ScRe$, $\Delta z/D_p = 1.0$. As the value of $ScRe$ decreases, the magnitude of $\Delta z/D_p$ decreases to a minimum at $ScRe \cong 2$, and then increases rapidly for lower values of $ScRE$. Using Eq. (1) or Fig. 2, the number of CSTR's connected in series can be defined by

$$N = \frac{L_b}{\Delta z} = \frac{m}{\pi R_b^2 D_p \rho_p (1 - \varepsilon_b)} \left(\frac{D_p}{\Delta z}\right) \tag{3}$$

During TPD, the desorbed gas diffuses through the pores of a particle until it reaches the exterior surface of the particle, where it is swept away by the flow of carrier gas. As the temperature of the bed increases, the carrier flow rate increases in

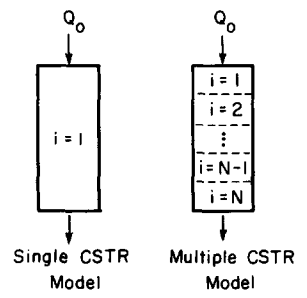

FIG. 1. Schematic of catalyst bed.

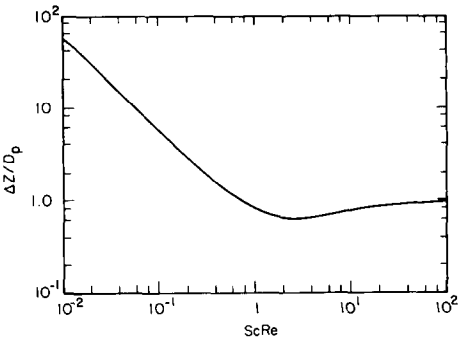

FIG. 2. Plot of $\Delta z/D_p$ versus $ScRe$.

accordance with the expression

$$Q = Q_0(T/T_0) \tag{4}$$

The temperature of the gas and solids in the bed are assumed to be equivalent and independent of bed position at all times. This allows a single temperature to be used to describe the desorption process. At any moment in time the temperature is given by

$$T = T_0 + \beta t \tag{5}$$

The desorption of gas within each CSTR is governed by three mass balances. The first, given by Eq. (6), describes the net loss of mass from the adsorption sites located within the pores of the catalyst particles.

$$\frac{\partial \theta_i}{\partial t} = nk_a C_{p,i}(1 - \theta_i)^n - nk_d \theta_i^n \tag{6}$$

The first term on the right-hand side of Eq. (6) describes the rate at which gas in the pores adsorbs onto vacant sites, while the second term on the right-hand side of Eq. (4) describes the rate of desorption from occupied sites. Notice that the equation is written for general nth order desorption kinetics. The rate coefficients k_a and k_d are functions of temperature and are represented by Eqs. (7) and (8)

$$k_a = s_0 \left(\frac{RT}{2\pi M}\right)^{1/2} \sigma \tag{7}$$

$$k_d = k_d^0 \exp(-E_d/RT) \tag{8}$$

The second mass balance is one written for a differentially thick spherical shell located within an individual catalyst particle. This is given by

$$\frac{\partial C_{p,i}}{\partial t} = \frac{D_e}{\varepsilon_p} \frac{1}{r^2} \frac{\partial}{\partial r}\left(r^2 \frac{\partial C_{p,i}}{\partial r}\right) - \frac{\rho_s}{n\varepsilon_p} \frac{\partial \theta_i}{\partial t} \tag{9}$$

The first term on the right-hand side of Eq. (9) describes the radial gradient in the diffusive flux, whereas the second term describes the net rate of desorption from sites located at radial position r inside a given particle. The effective diffusivity D_e is taken to be representative of Knudsen diffusion and is given by

$$D_e = D_k \varepsilon_p^2 = \frac{2}{3}\left(\frac{8RT}{\pi M}\right)^{1/2} d_p \varepsilon_p^2 \tag{10}$$

The initial condition for Eq. (9) is

$$C_{p,i} = 0 \qquad \text{for all } r \tag{11}$$

and the boundary conditions for Eq. (9) are

$$\frac{\partial C_{p,i}}{\partial r} = 0 \qquad \text{for } r = 0 \tag{12}$$

and

$$C_{p,i} = C_{b,i} \qquad \text{for } r = R_p \tag{13}$$

The third mass balance is that written for an individual CSTR and is represented by

$$\frac{\partial C_{b,i}}{\partial t} = \frac{NQ_0}{V\varepsilon_b} \frac{T}{T_0}(C_{b,i-1} - C_{b,i}) - \frac{3D_e}{R_p} \frac{(1 - \varepsilon_b)}{\varepsilon_b} \frac{\partial C_{p,i}}{\partial r}\bigg|_{r=R_p} \tag{14}$$

The first term on the right-hand side of this equation represents the net rate of removal of adsorbate by convection. The second term on the right-hand side describes the rate at which the adsorbate leaves the exterior surface of the catalyst particles. The initial condition for Eq. (14) is given by

$$C_{b,i} = C_b^0 \tag{15}$$

Equations (6), (9), and (14), together with the associated initial and boundary conditions, were solved numerically using a finite element, collocation technique developed for the solution of sets of partial differential equations. A description of the technique and the algorithm (PDECOL) may be found in Ref. (*8*).

RESULTS AND DISCUSSION

The model outlined in the preceding section was used to simulate the temperature-programmed desorption of CO and H_2 from a supported metal catalyst. The rate parameters used to describe the adsorption and desorption of both gases are given in Table 1 and are representative of values reported in the surface science literature for Group

TABLE 1

Parameter Values Used to Compute TPD Spectra

D_p	0.04–0.4 cm
m	12–108 mg
d_p	10^{-6} cm
ρ_s	9.77×10^{-5} mol/cm^3
σ	4.03×10^8 cm^2/mol
ε_p	0.70
ε_b	0.40
ρ_p	0.063 g/cm^3
s_0 for H_2	0.5
k_d^0 for H_2	10^{13} s^{-1}
E_d for H_2	18.0 kcal/mol
s_0 for CO	0.5
k_d^0 for CO	10^{15} s^{-1}
E_d for CO	30.0 kcal/mol

VIII metals (*9*). Also listed in Table 1 are the ranges examined for catalyst particle diameter, catalyst bed mass, and carrier gas flow rate. The values given are typical of those reported in a variety of experimental studies (*6*). The intraparticle and interparticle void fractions were also chosen to be representative but were maintained as fixed parameters. The diameter of the catalyst bed was chosen to be 1.0 cm and is characteristic of the internal diameter of many of the microreactors used in experimental studies of TPD (*6*). For an assumed particle diameter of 0.04 cm and a bed void fraction of 0.4, one particle layer corresponds to 12 mg of catalyst.

First-Order Kinetics

A series of calculations were performed using the rate parameters for CO given in Table 1, to assess the influence of readsorption and mass transfer effects on the position and shape of a TPD peak characteristic of a first-order desorption process. The catalyst mass was taken to be 25 mg, and the catalyst bed was treated as a single CSTR. For a particle diameter of 0.04 cm, a carrier gas flow rate of 1 cm^3/s, an initial uniform coverage of 1.0, and *assuming no readsorption,* the peak temperature and maximum desorption rate are 410 K and 2.64×10^{-2} s^{-1}, respectively. The ratio of the adsorbate concentration at the center to that at the surface of the particles, $C_p(0)/C_p(R_p)$, is equal to 1.14. Increasing the particle diameter to 0.4 cm and the carrier flow rate to 5.0 cm^3/s increases this ratio to 69.3; however, the peak temperature and maximum rate of desorption remain the same as those determined for the smaller radius and flow rate. These calculations show that in the absence of readsorption, the presence of very strong gradients in adsorbate concentration within the particles does not influence the characteristics of the TPD peak.

When readsorption is taken into account, the peak shifts to significantly higher temperatures and the maximum desorption rate decreases. Thus, for a particle diameter of 0.04 cm and a carrier flow rate of 1.0 cm^3/s, the peak maximum appears at 653 K and the maximum desorption rate is 8.8×10^{-3} s^{-1}. The extent to which readsorption influences the peak position and shape is comparable to that reported previously (*3–5*). It is noted further that, in contrast to what is observed in the absence of readsorption, the peak maximum temperature shifts from 653 to 673K as the initial CO coverage is decreased from 1.0 to 0.25. Shifts of a comparable magnitude have recently been reported by Jones and Griffin (*5*) for a first-order desorption process occurring in the presence of readsorption and intraparticle mass transfer.

Figure 3 shows a series of spectra determined for a 25 mg bed of catalyst consisting of particles with a diameter of 0.04 cm. As the carrier flow rate increases from 0.5 to 5 cm^3/s, the peak shifts to lower temperatures and becomes sharper. Table 2 shows that the gas concentrations at the center of the particles, $C_p(0)$, evaluated at the peak maximum temperature, decreases with increasing carrier flow rate but that $C_p(0)/C_p(R_p)$ increases. The observed trends can be explained in the following manner. With increasing carrier flow rate, the concentration of adsorbate in the voids between the particles, C_b, decreases. This causes $C_p(0)$ to de-

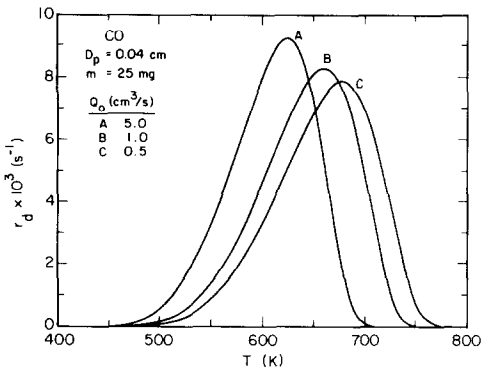

FIG. 3. Effect of carrier gas flow rate on TPD spectra for CO desorption: D_p = 0.04 cm; m = 25 mg.

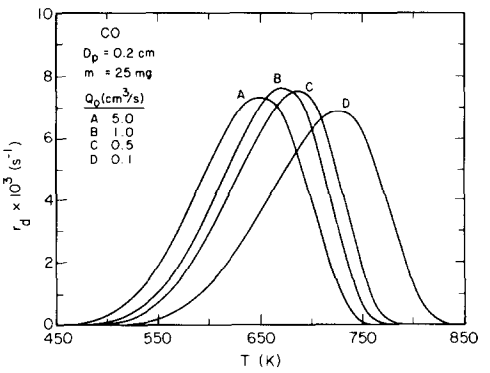

FIG. 4. Effect of carrier gas flow rate on TPD spectra for CO desorption: D_p = 0.20 cm; m = 25 mg.

crease and the gradient in C_p to increase. The decrease in the average value of C_p accelerates the net rate of desorption due to a suppression in the rate of adsorption, and is directly responsible for the shift in peak maximum temperature to lower values. It is significant to note that for all of the calculations presented in Fig. 3, the value of $\partial\theta_i/\partial t$ is many orders of magnitude smaller than the absolute rates of adsorption and desorption. This means that adsorption equilibrium is maintained throughout the course of TPD. Similar observations were also made for the other cases considered in this paper. Thus, consistent with the results reported by Herz *et al.* (*3*) and Gorte (*4*), equilibrium readsorption prevails under circumstances where a carrier gas is used to sweep away the desorbing adsorbate.

The effect of flow rate on the spectra for a 25 mg bed of catalyst consisting of 0.2-cm-diameter particles is shown in Fig. 4. The shift in peak temperature with carrier flow rate is less than that for the smaller particles, and the peak height passes through a maximum. The influence of flow rate on $C_p(0)$ and $C_p(0)/C_p(R_p)$ is given in Table 2. Here again, it is observed that the gas concentration within the particles decreases with increasing carrier flow rate. The principal difference with respect to the smaller particles (D_p = 0.04 cm) is that the decrease in the concentration at the center of the particles is significantly less than at the particle surface. If the carrier flow rate were increased to even higher levels (>5 cm³/s), a point would be attained where the position and shape of the TPD peak would no longer be sensitive to the flow rate. Under such circumstances, the removal of material from the catalyst particles would be completely dominated by intraparticle mass transfer. The appearance of a maximum in the peak height with increasing flow rate is due to the fact that the gas concentration in the pores reaches a maximum value at a temperature higher than that at which the bulk concentration in the carrier gas reaches its maximum. At high carrier flow rates, this effect causes an extension of the peak tail and a decrease in the peak height.

With increasing catalyst mass, and hence

TABLE 2

Values of $C_p(0)$ and $C_p(0)/C_p(R_p)$

Gas	D_p (cm)	m (mg)	Q_0 (cm³/s)	$C_p(0)$ (mol/cm³)	$C_p(0)/C_p(R_p)$
CO	0.04	25	0.5	1.00×10^{-9}	1.04
CO	0.04	25	1.0	5.66×10^{-10}	1.08
CO	0.04	25	5.0	1.72×10^{-10}	1.41
CO	0.20	25	0.1	4.81×10^{-9}	1.22
CO	0.20	25	0.5	1.90×10^{-9}	1.08
CO	0.20	25	1.0	1.47×10^{-9}	3.12
CO	0.20	25	5.0	1.07×10^{-9}	11.45
CO	0.04	12	1.0	3.16×10^{-10}	1.17
CO	0.04	12	5.0	1.15×10^{-10}	1.85
CO	0.20	12	5.0	1.23×10^{-9}	22.81
H_2	0.04	12	1.0	1.77×10^{-9}	1.15
H_2	0.04	12	5.0	6.31×10^{-10}	1.70

bed depth, axial gradients in C_b can develop along the bed. The extent to which this is important is governed by the value of $ScRe$. When a significant axial concentration gradient is anticipated, it is no longer appropriate to model the bed as a single CSTR, and use of the multiple CSTR model is required. Table 3 illustrates how the value of N changes with catalyst mass and carrier gas composition, and Fig. 5 shows how these variables influence the TPD spectrum for CO.

For a catalyst mass of 12 mg, the spectra are the same regardless of carrier gas composition. The reason is that, as indicated in Table 3, $N = 1$ in both cases. When the catalyst mass is increased to 108 mg, N continues to be 1.0 if the carrier is helium, but increases to 9.0 if the carrier is argon. Figure 5 shows that in this instance the carrier gas composition does have an influence on both the position and shape of the spectrum. It is also significant to note that in both cases, the peak maximum is shifted to higher temperatures relative to the peak maximum observed when 12 mg of catalyst are used. The observed upscale shift in peak position is due to the increase in the average value of C_b in the bed.

The axial distribution of gas through the bed for Case B in Fig. 5 is shown in Fig. 6. For the sake of clarity, the points representing the gas composition at the exit from each CSTR have been connecting by straight line segments. As can be seen, the concentration profile changes radically as

TABLE 3

Effects of Experimental Conditions on the Number of CSTR's Required to Model the Catalyst Bed

Carrier gas	Q_0 (cm³/s)	D_p (cm)	m (mg)	$\frac{L_b}{D_p}$	$\frac{\Delta z}{D_p}$	N
He	2	0.04	12	1	12.29	1
Ar	2	0.04	12	1	0.90	1
He	2	0.04	108	9	12.29	1
Ar	2	0.04	108	9	0.90	9

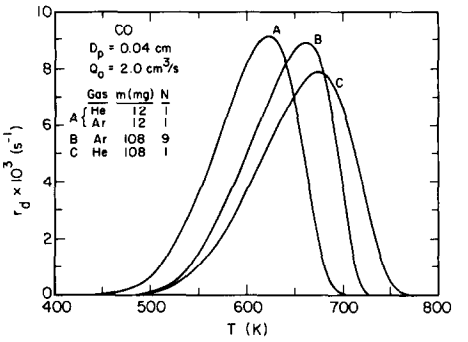

FIG. 5. Effect of catalyst mass and carrier gas composition on TPD spectra for CO desorption: $D_p = 0.04$ cm; $Q_0 = 2.0$ cm³/s.

desorption proceeds. For temperatures below 660 K, the profile is convex, but above 660 K, the profiles becomes concave. It is also apparent that the maximum in the local value of C_b with increasing temperature depends on the axial position in the bed.

For a gas such as CO, the initial sticking coefficient and the binding energy are high enough that adsorption at ambient temperatures will occur as a chromatographic front which gradually penetrates into the interior of each catalyst particle. If the bed is several particle-diameters deep, then the propagation of a front in the axial direction of

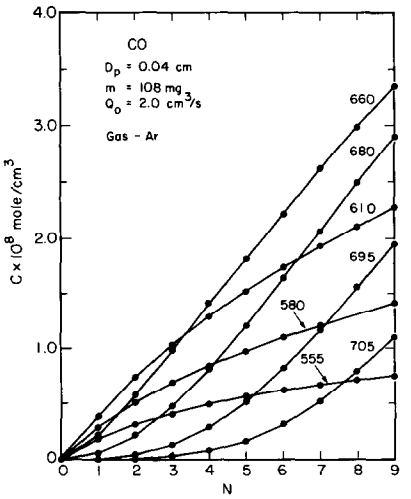

FIG. 6. Gas phase concentration in each particle layer for different bed temperatures: $D_p = 0.04$ cm; $m = 108$ mg; $Q_0 = 2.0$ cm³/s.

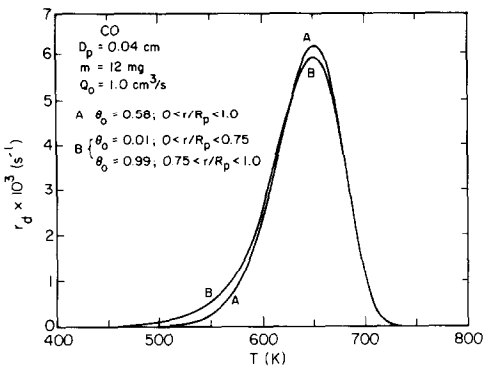

FIG. 7. Comparison of TPD spectra for uniform and nonuniform initial adsorption of CO: D_p = 0.04 cm; m = 12 mg; Q_0 = 1.0 cm³/s.

the bed is also expected. Figures 7 and 8 present results for two cases. In the first, it is assumed that a uniform initial coverage of 0.58 prevails across the radius of all particles contained in a 12-mg bed. In the second case, it is assumed that the average initial loading of CO is the same but that the distribution is such that adsorption sites contained in the outer 25% of the particle radius are nearly saturated while those in the interior 75% of the particle radius are almost totally vacant. Figure 7 shows that the TPD spectra for the two cases are quite similar. The only differences are that the spectrum for the case of nonuniform initial distribution begins at somewhat lower temperatures and exhibits a somewhat smaller peak. The areas under the two curves, however, are the same, since the initial adsorbate loading is the same. The change in the distribution of adsorbate surface coverage with temperature is shown in Fig. 8 for the case of nonuniform initial adsorption. It is apparent that as the temperature increases the nonuniformity in the profile is rapidly smoothed out. Comparison of Figs. 7 and 8 shows that a nearly uniform distribution is achieved by 600 K, a temperature well below that for which a significant fraction of the initial adsorbate has been removed. It is significant to observe that for particles much larger than 0.04 cm in diameter, a significantly greater fraction of the initially adsorbed gas would be lost before a uniform distribution was achieved. This would contribute to a greater difference in the shapes of the TPD spectra for uniform and nonuniform adsorbate distribution, than that seen in Fig. 7. A greater effect of nonuniform initial adsorbate distribution would also be expected for high carrier gas flow rates. Under such conditions, the diffusion of adsorbate from the portions of the particles near the outer surface of the particles will be very rapid. This will cause a substantial amount of adsorbate to be depleted from the interior of the particle before the initial nonuniformity can be annealed by intraparticle diffusion.

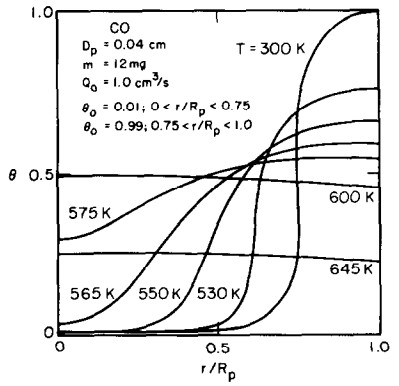

FIG. 8. Coverage profiles for different temperatures during TPD for an initially nonuniform adsorption of CO: D_p = 0.04 cm; m = 12 mg; Q_0 = 1 cm³/s.

Second-Order Desorption Kinetics

A series of calculations were also performed for an adsorption–desorption process obeying second-order kinetics. The rate parameters used for these calculations are given in Table 1 and were selected to be representative of those for the adsorption and desorption of H_2 from Group VIII metals (*9*). Figure 8 illustrates the effect of changes in the initial coverage on the TPD spectra, under the assumption that the coverage is uniformly distributed from the outset. As would be expected for second-order desorption kinetics, the peak temperature

shifts to higher values as the initial coverage decreases.

Figure 9 illustrates the effects of flow rate on the TPD spectra calculated for a bed of particles 0.04 cm in diameter. Increasing the carrier flow rate from 1.0 to 5.0 (STP) cm^3/s causes a 25 K downscale shift in the peak maximum temperature. The reasons for this are identical to those presented in the discussion concerning the calculations for first-order desorption kinetics. Table 2 again shows that with increasing carrier flow rate, the gas phase concentration of adsorbate in the particle pores decreases, thereby reducing the rate of readsorption.

The effects of a nonuniform initial adsorbate coverage is shown in Fig. 10. The results are essentially the same as those for the first-order process, except that for second-order desorption kinetics, the peak location shifts to slightly higher temperatures as a consequence of nonuniformities in the initial adsorbate coverage. While not shown, it was observed that the distribution of surface coverage becomes uniform before an appreciable amount of adsorbate desorbs.

Determination of Rate Parameters from TPD Spectra

In the absence of mass transfer effects, and assuming equilibrium adsorption, the heat of adsorption, ΔH, and the ratio of

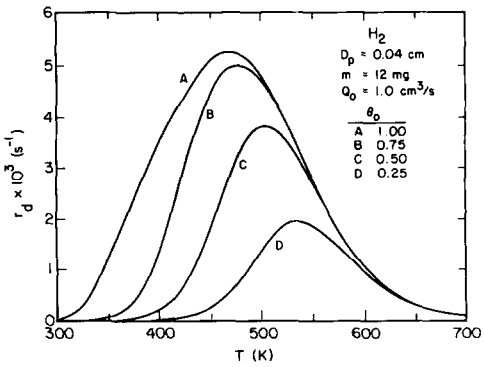

FIG. 9. Effect of initial coverage on TPD spectra for H_2 desorption: D_p = 0.04 cm; m = 12 mg; Q_0 = 1.0 cm^3/s.

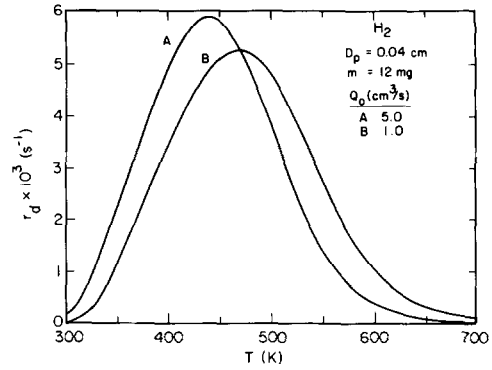

FIG. 10. Effect of carrier gas flow rate on TPD spectra for H_2 desorption: D_p = 0.04 cm; m = 12 mg; Q_0 = 1.0 cm^3/s.

preexponential factors for adsorption and desorption, A, can be determined from the expression (*1, 2*)

$$\ln\left[\frac{\theta_m^{n-1}T_m^2}{(1-\theta_m)^{n+1}\beta}\right] = \frac{\Delta H}{RT_m} + \ln\left[\frac{V_a\Delta H}{QnAR}\right] \quad (16)$$

Variations in T_m and θ_m are usually achieved by varying the heating rate, β, and/or the initial coverage of adsorbate. A straight line is obtained by plotting the left-hand side of Eq. (16) versus T_m^{-1}. Values for ΔH and A can then be determined from the slope and intercept of this line. Under the assumption that adsorption is not activated, $E_d = \Delta H$, and the preexponential factor for desorption is given by $k_d^0 = k_A/A$.

For all of the cases considered here, equilibrium adsorption was very closely approximated throughout the course of TPD. This observation motivated an assessment of the applicability of Eq. (16) for determining E_d and k_d^0 in the presence of significant mass transfer effects. Figure 11 and Table 4 show the results obtained for the first-order desorption of CO. Three cases are considered. In Case 1a, there are no radial concentration gradients in the catalyst particles and the bed is small enough for there to be no axial concentration gradients. Case 2a corresponds to a situation in which significant radial concentration gradients will oc-

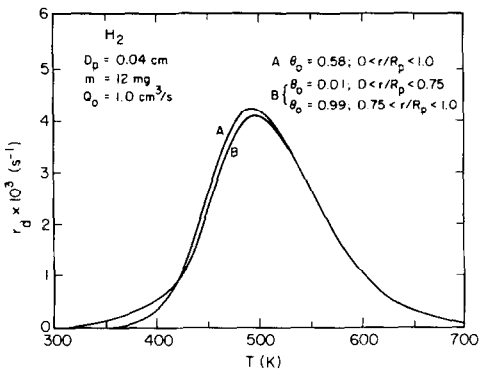

FIG. 11. Comparison of TPD spectra for uniform and nonuniform initial adsorption of H_2: D_p = 0.04 cm; m = 12 mg; Q_0 = 1.0 cm^3/s.

cur within the catalyst particles but none in the axial direction. In Case 3a, there are severe axial gradients but no radial gradients within the particles. The presence or absence of axial gradients depends on the carrier gas composition. If the carrier gas is helium, then there is no axial gradient, but if the carrier gas is argon, a significant axial gradient will be present (see Fig. 6). Figure 11 shows that in each case a plot of Eq. (16) produces a straight line. For Case 1a, Table 4 shows that the activation energy for desorption determined from the slope of Eq. (16) differs from 30 kcal/mol by only 1.3%. The preexponential factor for desorption, however, differs from 10^{15} s^{-1} by 200%. In Case 2a, the error in the estimated value of E_d increases to 3.3% and that in k_d^0 to 30%.

TABLE 4

Values of k_d^0 and E_d Determined from Eq. (16)

Case	Adsorbate	D_p (cm)	m (mg)	Q_0 (cm^3/s)	k_d^{0c} (s^{-1})	E_d^d (kcal/mol)
1a	CO	0.04	12	1.0	3×10^{15}	30.4
2a	CO	0.20	12	5.0	7×10^{14}	31.0
3a	CO	0.04	108	2.0[a]	5×10^{15}	31.0
3a	CO	0.04	108	2.0[b]	9×10^{16}	33.0
1b	H_2	0.04	12	1.0	3×10^{13}	18.5
2b	H_2	0.04	12	5.0	2×10^{13}	18.4

[a] Assuming that the carrier gas is helium; N = 1.
[b] Assuming that the carrier gas is argon; N = 9.
[c] The correct value for k_d^0 is 10^{15} s^{-1} for CO and 10^{13} s^{-1} for H_2.
[d] The correct value for E_d is 30 kcal/mol for CO and 18 kcal/mol for H_2.

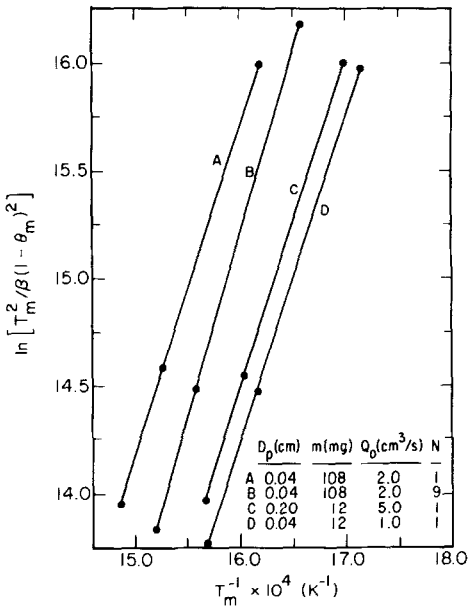

FIG. 12. Plot of $\ln[T_m^2/(1-\theta_m)^2\beta]$ versus T_m^{-1} for CO desorption.

If helium is the carrier gas for Case 3a, then the error in E_d is 3.3% and that in k_d^0 is 400%, but if the carrier gas is argon, the error in E_d rises to 10.0% and that in k_d^0 to 8900%.

Estimates of E_d and k_d^0 using Eq. (16) were also carried out for desorption of H_2. Table 4 shows that for Case 1b, in which there are no radial or axial concentration gradients, the error in the estimate of E_d is 2.8% and the error in the estimate of k_d^0 is 300%. In Case 2b, strong gradients occur across the radius of each particle, but none in the axial direction of the bed. Table 4 shows that in this instance the error in the estimate of E_d decreases to 2.2% and the error in the estimate of k_d^0 decreases to 200%.

Criteria for the Absence of Intraparticle Mass Transfer Effects

Two attempts have recently been made to define criteria for the absence of intraparticle mass transfer effects during TPD in the presence of readsorption. Ibok and Ollis (*10*) have proposed that these effects will be negligible provided the following in-

equality is satisfied

$$R_p < \left[\left(\frac{D}{1+K}\right)\frac{\alpha C_b|_{T_m}}{\beta k \rho_s (d\theta/dT)|_{T_m}}\right]^{1/2} \quad (17)$$

This relationship was derived by ad hoc modification of the Weisz–Prater (*11*) criterion for the absence of intraparticle mass-transfer effects during steady-state reaction. Evaluation of Eq. (17) for the conditions of Case 1a in Table 4 gives $R_p < 5.7 \times 10^{-4}$. Since $C_p(0)/C_p(R_p) = 1.04$ for this case, where $R_p = 0.02$ cm, it is apparent that the criterion given by Eq. (17) is more stringent than necessary.

Gorte (*4*) has proposed that intraparticle concentration gradients are negligible provided the following inequality is satisfied

$$\frac{QR_p}{D_e S} = \frac{Q\rho_p R_p^2}{3mD_e} < 1 \quad (18)$$

This criterion was obtained by nondimensionalization of the differential equations governing mass transfer during TPD. In applying Eq. (18), it must be assumed that the average residence time of gas in the TPD reactor is much smaller than the time required to heat the reactor from its initial to final temperature. This condition is easily satisfied in most experimental situations (*4*), including that described in the present paper. Application of Gorte's criterion to two of the cases considered here gives the following results. For CO desorption from a 25-mg catalyst bed made up of 0.04-cm-diameter particles, and assuming a carrier flow rate of 0.5 cm^3/s, the value of the group on the left-hand side of Eq. 18 is 0.3. Table 2 shows that for these conditions $C_p(0)/C_p(R_p) = 1.04$ and, hence, that the intraparticle concentration gradient is small. When $R_p = 0.1$ cm and $Q = 5$ cm^3/s, the left-hand side of Eq. (18) becomes 80. The value of $C_p(0)/C_p(R_p)$ in this case is 11.5, indicating the presence of a strong intraparticle concentration gradient. These calculations demonstrate that the criterion proposed by Gorte (*4*) provides a sound basis for predicting the onset of severe intraparticle mass transfer effects. This result is perhaps not surprising given that Gorte's criterion was derived by proper dimensional analysis of the physical problem.

CONCLUSIONS

The results of the analysis presented here demonstrate that the position and shape of TPD spectra obtained from porous catalysts are sensitive functions of catalyst particle size, catalyst bed depth, carrier flow rate, and carrier gas composition. Similar effects are observed for first- and second-order adsorption–desorption kinetics. Extensive readsorption of gas occurs within the catalyst particles and the local adsorbate coverage is governed by equilibrium adsorption. Intraparticle concentration gradients can be minimized by reducing catalyst particle size and carrier flow rate. The criterion for negligible intraparticle concentration gradients proposed by Gorte (*4*) is found to be valid. Axial gradients in the gas phase concentration of adsorbate can be minimized by the use of very shallow catalyst beds. The bed depth over which the gas composition may be regarded as uniform is a function of *ScRe*. For small particles (e.g., $D_p = 0.04$ cm), nonuniform initial adsorption profiles are rapidly annealed upon heating of the catalyst, prior to significant loss of adsorbate from the particles. As a consequence, the TPD spectra for nonuniform initial adsorption and uniform initial adsorption are quite similar. Reasonably accurate estimates of the enthalpy of adsorption can be obtained using a theoretical relationship based on the assumption of equilibrium adsorption in the absence of intraparticle or interparticle gradients in adsorbate concentration. Use of this relationship to determine the preexponential factor for desorption produces large errors when significant mass transfer effects are present.

APPENDIX: NOMENCLATURE

A ratio of preexponential factors for adsorption and desorption (mol/cm^3)

$C_{b,i}$ gas phase concentration of adsorbate in the ith CSTR (mol/cm^3)
C_b^0 initial value of gas phase concentration of adsorbate (mol/cm^3)
$C_{p,i}$ gas phase concentration of adsorbate in the pores of particles in the ith CSTR (mol/cm^3)
$\mathscr{D}$ molecular diffusion coefficient (cm^2/s)
D_e effective diffusion coefficient (cm^2/s)
D_k Knudsen diffusion coefficient (cm^2/s)
D_p particle diameter (cm)
d_p average pore diameter (cm)
E_d activation energy for desorption (kcal/mol)
ΔH heat of adsorption (kcal/mol)
K adsorption equilibrium constant
k_a rate coefficient for adsorption (cm^3/mol · s)
k_d rate coefficient for desorption (s^{-1})
k_d^0 preexponential factor for desorption (s^{-1})
L_b length of catalyst bed (cm)
M molecular weight of adsorbate (g/mol)
m catalyst mass (mg)
N number of CSTR's used to represent the catalyst bed
n reaction order
Pe Peclet number, $\bar{u}D_p/\mathscr{D}$
Q volumetric flow rate of carrier gas at temperature T (cm^3/s)
Q_0 volumetric flow rate of carrier gas at temperature T_0 (cm^3/s)
R gas constant (atm cm^3 mol^{-1} K^{-1})
R_b bed radius (cm)
Re Reynolds number, $\rho_g\bar{u}D_p/\mu_g$
R_p particle radius (cm)
r radial position (cm)
S total external area of catalyst particles (cm^2)
Sc Schmidt number, $\mu_g/\rho_g\mathscr{D}$
s_0 initial sticking coefficient
T temperature (K)
T_m peak maximum temperature (K)
T_0 initial catalyst temperature (295 K)
t time (s)
$\bar{u}$ average linear velocity (cm/s)
V total volume of catalyst (cm^3)
V_a total volume of adsorption sites (mol)

α $C_p(0)/C_b$
β heating rate (K/s)
ε_b catalyst bed void fraction
ε_p catalyst particle void fraction
μ_g gas viscosity (g/cm · s)
ρ_g gas density (g/cm^3)
ρ_p catalyst density (g/cm^3)
ρ_s concentration of adsorption sites in a catalyst particle (mol/cm^3)
σ area of adsorption sites (cm^2/mol)
θ_i fractional coverage of adsorption sites in the ith CSTR
θ_m fractional coverage of adsorption sites at T_m

ACKNOWLEDGMENTS

This work was supported by the Division of Chemical Sciences, Office of the Basic Energy Sciences, U.S. Department of Energy under Contrast DE-AC03-76SF 00098 and by the Engineering Directorate of the National Science Foundation under Grant CPE-7826352.

REFERENCES

1. Cvetanovic, R. J., and Amenomiya, Y., "Advances in Catalysis," Vol. 17, p. 103. Academic Press, New York. 1967.
2. Cvetanovic, R. J., and Amenomiya, Y., *Catal. Rev.* **6,** 21 (1972).
3. Herz, R. K., Kiela, J. B., and Marin, S. P., *J. Catal.* **73,** 66 (1982).
4. Gorte, R. J., *J. Catal.* **75,** 164 (1982).
5. Jones, D. M., and Griffin, G. L., *J. Catal.* **80,** 40 (1983).
6. Falconer, J. L., and Schwartz, J. A., *Catal. Rev. Sci. Eng.* **25,** 141 (1983).
7. Butt, J. B., "Reaction Kinetics and Reactor Design." Prentice–Hall, Englewood Cliffs, N.J., 1980.
8. Madsen, N. K., and Sincovec, R. F., *Assoc. Comput. Mach. Trans. Math. Software* **5,** 326 (1979).
9. Somorjai, G. A., "Chemistry in Two Dimensions: Surfaces," Cornell Univ. Press, Ithaca, N.Y., 1981.
10. Ibok, E. E., and Ollis, D. F., *J. Catal.* **66,** 391 (1980).
11. Weisz, P. B., and Prater, C. D., "Advances in Catalysis," Vol. 6, p. 143. Academic Press, New York, 1954.